

Investigating the thermal conductivity of materials by analyzing the temperature distribution in diamond anvils cell under high pressure

Caihong Jia(贾彩红), Min Cao(曹敏), Tingting Ji(冀婷婷), Dawei Jiang(蒋大伟), and Chunxiao Gao(高春晓)

Citation: Chin. Phys. B, 2022, 31 (**4**): 040701. DOI: 10.1088/1674-1056/ac29aa
Journal homepage: http://cpb.iphy.ac.cn; http://iopscience.iop.org/cpb

What follows is a list of articles you may be interested in

A new technology for controlling *in-situ* oxygen fugacity in diamond anvil cells and measuring electrical conductivity of anhydrous olivine at high pressures and temperatures

Wen-Shu Shen(沈文舒), Lei Wu(吴雷), Tian-Ji Ou(欧天吉), Dong-Hui Yue(岳冬辉), Ting-Ting Ji(冀婷婷), Yong-Hao Han(韩永昊), Wen-Liang Xu(许文良), Chun-Xiao Gao(高春晓)
Chin. Phys. B, 2020, 29 (**1**): 010702. DOI: 10.1088/1674-1056/ab5934

Thermal characterization of GaN heteroepitaxies using ultraviolet transient thermoreflectance

Kang Liu(刘康), Jiwen Zhao(赵继文), Huarui Sun(孙华锐), Huaixin Guo(郭怀新), Bing Dai(代兵), Jiaqi Zhu(朱嘉琦)
Chin. Phys. B, 2019, 28 (**6**): 060701. DOI: 10.1088/1674-1056/28/6/060701

Magnetic field analysis in a diamond anvil cell for Meissner effect measurement by using the diamond NV^- center

Lin Zhao(赵琳), Donghui Yue(岳冬辉), Cailong Liu(刘才龙), Min Wang(王敏), Yonghao Han(韩永昊), Chunxiao Gao(高春晓)
Chin. Phys. B, 2019, 28 (**3**): 030702. DOI: 10.1088/1674-1056/28/3/030702

Pressure-induced phase transition of B-type Y_2O_3

Qian Zhang(张倩), Xiang Wu(巫翔), Shan Qin(秦善)
Chin. Phys. B, 2017, 26 (**9**): 090703. DOI: 10.1088/1674-1056/26/9/090703

Magnetic transition of ferromagnetic material at high pressure using a novel system

Hu Tian-Li, Wang Xin, Han Bing, Li Yan, Huang Feng-Xian, Zhou Qiang, Zhang Tao
Chin. Phys. B, 2013, 22 (**12**): 120701. DOI: 10.1088/1674-1056/22/12/120701

Investigating the thermal conductivity of materials by analyzing the temperature distribution in diamond anvils cell under high pressure

Caihong Jia(贾彩红)[1,2], Min Cao(曹敏)[1], Tingting Ji(冀婷婷)[1], Dawei Jiang(蒋大伟)[1], and Chunxiao Gao(高春晓)[1,†]

[1] *State Key Laboratory of Superhard Materials, Jilin University, Changchun* 130000, *China*
[2] *College of Mathematics and Physics, Inner Mongolia University for Nationalities, Tongliao* 028043, *China*

(Received 6 July 2021; revised manuscript received 27 August 2021; accepted manuscript online 24 September 2021)

Investigating the thermal transport properties of materials is of great importance in the field of earth science and for the development of materials under extremely high temperatures and pressures. However, it is an enormous challenge to characterize the thermal and physical properties of materials using the diamond anvil cell (DAC) platform. In the present study, a steady-state method is used with a DAC and a combination of thermocouple temperature measurement and numerical analysis is performed to calculate the thermal conductivity of the material. To this end, temperature distributions in the DAC under high pressure are analyzed. We propose a three-dimensional radiative–conductive coupled heat transfer model to simulate the temperature field in the main components of the DAC and calculate *in situ* thermal conductivity under high-temperature and high-pressure conditions. The proposed model is based on the finite volume method. The obtained results show that heat radiation has a great impact on the temperature field of the DAC, so that ignoring the radiation effect leads to large errors in calculating the heat transport properties of materials. Furthermore, the feasibility of studying the thermal conductivity of different materials is discussed through a numerical model combined with locally measured temperature in the DAC. This article is expected to become a reference for accurate measurement of *in situ* thermal conductivity in DACs at high-temperature and high-pressure conditions.

Keywords: thermal conductivity, heat radiation effect, temperature field, diamond anvil cell

PACS: 07.35.+k, 47.11.Df, 51.20.+d, 61.80.–x **DOI:** 10.1088/1674-1056/ac29aa

1. Introduction

Currently, the diamond anvil cell (DAC) is the only static high-pressure device that can generate an environment with a pressure as high as 1 million atmospheres.[1–3] In combination with electrical, optical, magnetic, mechanical and other methods to measure physical properties, a DAC can characterize material structure and various physical properties under high pressure.[4–8] Accordingly, DACs have been widely applied in diverse fields including materials science, physics and chemistry.[9–14] When a DAC is subjected to high temperatures it can simulate the conditions in the earth's interior in the laboratory, which is of great importance for investigating the thermal properties of minerals and rocks.[15–17] However, it is an enormous challenge to characterize the thermophysical properties of the material under test at conditions of extremely high temperature and high pressure (HT–HP).[18] This challenge is even more pronounced in the DAC platform.

Currently, the thermal transport properties of materials in a DAC are mostly studied through the laser flash method.[19–23] However, this method has some disadvantages, such as the technological challenges involved in preparing samples. In order to accurately measure the heat transport properties of materials under extreme conditions, innovations have been proposed to measure the steady-state heat conductivity of materials through a DAC.[17] The main idea in this regard was to realize the temperature gradient of samples by directly heating the upper and lower diamond anvils (DAs) in a high-temperature resistant furnace. Therefore, it is essential to calculate the temperature distributions in the sample to study the *in situ* heat transport properties in the DAC. To this end, replace contact temperature measurement is often used in the steady-state method. It is worth noting that because of the high thermal conductivity of diamond it can be regarded as a thermostatic substance. Accordingly, the temperature of the diamond side edge measured by the thermocouple can be used as the temperature of the sample surface. Despite the remarkable advantages of this method, it cannot directly measure the temperature of the sample surface. Meanwhile, further investigations into the reliability of the replace contact temperature measurement method should be carried out when a temperature gradient exists in the anvil itself. In this regard, Yue *et al.* showed that conventional contact temperature measurement inevitably produces experimental errors that cannot be ignored. Accordingly, they combined the finite element method with multi-thermocouple local temperature measurement and analyzed the temperature distribution in the anvil and sample.[17] Accordingly, it was found that the outer wall of the DAC radiates heat to the surrounding flow through surface radiation, and the heat loss caused by surface radiation significantly affects the temperature field distribution in the DAC.

†Corresponding author. E-mail: cc060109@qq.com
© 2022 Chinese Physical Society and IOP Publishing Ltd

Diamond can be considered a translucent medium. Since heat rays can penetrate deep into the material, the transmission of a semitransparent medium is different from that of most solid materials.[24] Based on this hypothesis, there is not only heat conduction in the anvil but also heat absorption, re-emittance and energy scattering within the anvil volume.[25] Therefore, heat transfer is quite a complex phenomenon in a DAC under stable heating conditions. A review of the literature indicates that the influence of radiant heat on the temperature field of the main components of a DAC is usually neglected.

In the present study, we aim to realize the temperature gradient distribution of the sample by directly heating the upper and lower bases of DAs in a high-temperature resistant furnace. In order to accurately measure the *in situ* thermal conductivity of the sample in the DAC under HT–HP conditions, a radiative–conductive coupled heat transfer model is proposed to analyze the heat transfer in key components of the DAC under stable heating conditions. It is worth noting that the influence of the radiation effect on the temperature distribution of the DAC can be simulated through numerical methods. The main purpose of the present study is to investigate the feasibility of thermal conductivity measurement by combining numerical simulation and local temperature measurement of thermocouples in DAs at high pressures. This study is expected to provide a reference for the accurate measurement of *in situ* thermal conductivity in a DAC under HT–HP conditions.

2. Numerical method

The geometric structure of the diamond anvils, gasket and sample (DAGS) was modeled in accordance with the experiment. Figure 1 illustrates the prepared model. In the experiment, type Ia diamond was used as the anvil. In order to realize the temperature gradient distribution of samples in the DAC, the anvil was fixed on a high-temperature seat. Considering the high thermal conductivity of diamond, the base of the anvil can be regarded as an isothermal surface. In this regard, T_1 and T_2 denote the temperatures of the upper and lower anvil bases, respectively. Moreover, T_3 and T_4 are the temperatures at the midpoint of the lateral edges of the upper and lower diamond anvils D_3 and D_4, respectively. T_1–T_4 reflect the measured temperatures from four thermocouples.

In the present study, the DAC device is equipped with a vacuum facility to ensure a vacuum degree of 1 Pa around the DAC. A vacuum environment effectively eliminates air conduction and convection. On the other hand, thermal radiation efficiency is highest in a vacuum environment.[26] Therefore, it is necessary to consider the influence of the radiation effect on the temperature distribution in the DAC. Meanwhile, heat energy transfers from the upper and lower translucent anvil bases to the sample in the pressure chamber through conduction and radiation mechanisms.

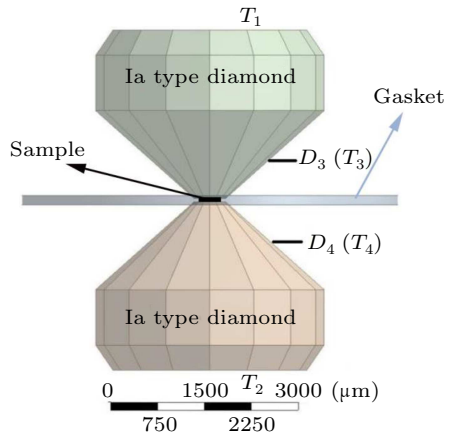


Fig. 1. Schematic configuration of the diamond anvils, gasket and sample. T_1–T_4 are the measured temperatures from four thermocouples.

In the present study, a coupled radiative–conductive heat transfer model was developed based on the finite volume method (FVM) to simulate the temperature and heat flow field distributions in the DAGS. The proposed model fully considers the effects of radiation heat transfer in the diamond on the temperature distribution. Since the thermal radiation is highly localized, the sensitivity of angular discretization should be considered in the calculations. The heat flux of the wall results in non-physical oscillation in large discretization dispersion in the angular coordinate. As the angular discretization increases, the heat flow gradually becomes smooth. In this scheme, the *in situ* thermal conductivity of the sample is studied by combining numerical analysis and the locally measured temperatures via thermocouples in the DAC. In this regard, four thermocouples were arranged at the middle point of the side edge and the base of the upper and lower DAs.

In the calculations, the temperature boundary conditions of the upper and lower bases of the DAs are assumed to be T_1 and T_2, respectively. Under a certain temperature boundary, the coupled radiative–conductive heat transfer model is used to simulate the temperature gradient of the sample in the DAC under HT–HP conditions. In all calculations, it is assumed that the thermal conductivity of the sample changes until the calculated temperatures t_3' and t_4' at the midpoints D_3, D_4 of the lateral edges of the DAs reach the measured temperatures T_3 and T_4. In our previous study, a combination of temperature measurement through thermocouples and numerical analysis was realized to calculate the thermal conductivity of the sample in the DAC in the absence of radiation heat transfer.[17] Then this method was verified via the characterization of the thermal conductivity of diamond.[28] It was found that, as the diamond temperature increases, the influence of the radiation on the temperature field of the DAC increases. Since the radiation–conduction heat transfer model is applied to analyze the heat fluxes, it is necessary to know the radiant characteristics of a Iatype diamond anvil. Tables 1 and 2 present the heat radiation characteristics and thermodynamic parameters of the DAGS used in the analysis.

Table 1. Radiant characteristics of Ia-type diamond.

Band (nm)	Emissivity	Absorption coefficient (cm^{-1})	Refractive index
200–470	0.28	1.83	1.95
470–580	0.15	0.56	1.96
580–2500	0.1	0.23	1.97
2500–3703	0.24	2.23	2.3
3703–6667	0.55	14.68	2.4
6667–9550	0.6	46.67	2.4
9550–10848	0.65	19.77	2.45
10848–50000	0.57	12.73	2.4

Table 2. Thermodynamic parameters of materials used in numerical simulation.

Property	Diamond	Sample	Spacer
Density (kg/m^3)	3520	3000	7000
Thermal conductivity ($W{\cdot}m^{-1}{\cdot}K^{-1}$)	function of temperature[28]	2	17[27]
Specific heat capacity ($J{\cdot}kg^{-1}{\cdot}K^{-1}$)	function of temperature[29]	420	460

3. Result and discussion

In order to accurately measure the *in situ* thermal conductivity in the DAC under HT–HP conditions, a radiation–conduction coupling model was developed to study the influence of the radiation effect on the heat flow field of the DAC. When the mode of heat transfer in the DAC had been determined, the thermal conductivity of different materials under high pressure was studied with locally installed thermocouples at the boundaries.

3.1. Influence of the radiative effect on the heat transfer of the DAC

The DAC device was equipped with a vacuum housing to prevent convection of heat from the surrounding air. However, heat radiation intensifies in a vacuum environment. In order to evaluate the radiation effect on the temperature distribution in the DAC, the radiation–conduction coupling heat transfer model was used to quantitatively analyze the influence of radiation on the temperature and heat flow of the DAGS. The radiation consists of two parts, including the radiant heat loss on the outer wall of the DAC in the vacuum environment and the transmission and absorption of radiation inside the solid region of the DAs.

The presence of heat radiation leads to heat loss in the DAC, thereby decreasing the overall temperature. In all simulations, T_1 and T_2 of the DA bases and the sample conductivity were set to 873 K, 943 K, and 2 $W{\cdot}m^{-1}{\cdot}K^{-1}$, respectively. Based on the radiation–conduction coupling heat transfer model, the heat transfer mechanism in the anvil and sample is confined to the radiation effect. Figure 2(a) indicates that the temperature and heat flow of the sample reduce to 2.38 K–2.60 K and 82 $W{\cdot}m^{-2}$–14785 $W{\cdot}m^{-2}$, respectively. Moreover, figure 2(b) reveals that the temperature decreases on the upper and lower walls of the sample. Figure 2(b) indicates that the temperature of the upper wall of the sample and the heat flux difference decrease to 2.44 K–2.59 K, and 6940 $W{\cdot}m^{-2}$–8520 $W{\cdot}m^{-2}$, respectively. Furthermore, the temperature of the lower wall and the heat flux decrease to 2.38 K–2.51 K and 90 $W{\cdot}m^{-2}$–1110 $W{\cdot}m^{-2}$, respectively. Figure 2(e) shows that the temperature of DAs along the lateral edges and the heat flux decrease to 0.3 K–3.06 K and 25276 $W{\cdot}m^{-2}$–34251 $W{\cdot}m^{-2}$, respectively. Accordingly, it is found that radiation is the dominant heat transfer mechanism in the entire flow field and affects the axial (longitudinal) temperature gradient. Studies show that thermal radiation dominates in the heat transfer process for materials with an extinction coefficient less than 20 cm^{-1} at temperatures higher than 600 K.[30] Accordingly, the proportion of radiation heat transfer to total heat transfer increases as the temperatures of the bases of DAs T_1 and T_2 increase. It is observed that ignoring the radiant heat transfer leads to a large error in the DAC under HT–HP conditions. The proposed radiation–conduction coupling model is closer to the actual heat transfer in the DAC, which sufficiently considers the influence of heat radiation on the accurate *in situ* measurement of the thermal conductivity of materials.

3.2. Measurement of thermal conductivity by analyzing the temperature field in the DAC

In measuring the thermal conductivity of samples in the DAC at high pressures, the temperatures T_1 and T_2 of the upper and lower anvil bases are applied in the finite volume simulation as temperature boundary conditions. The sample temperature gradient in the DAC is simulated by the radiation–conduction coupling heat transfer model at HT–HP conditions. The obtained results reveal that for different thermal conductivities of the sample, the calculated temperatures t_3' and t_4' are consistent with the measured temperature from thermocouples at the midpoint positions D_3 and D_4 of the DAs. The input thermal conductivity reflects the thermal conductivity of

the sample under this pressure. In other words, the thermal conductivity of the sample affects the temperature distribution in the DAC. In the proposed model, the thermal conductivity of the sample was determined by detecting the temperature change of the midpoint positions D_3 and D_4 of the side edges of the anvils.

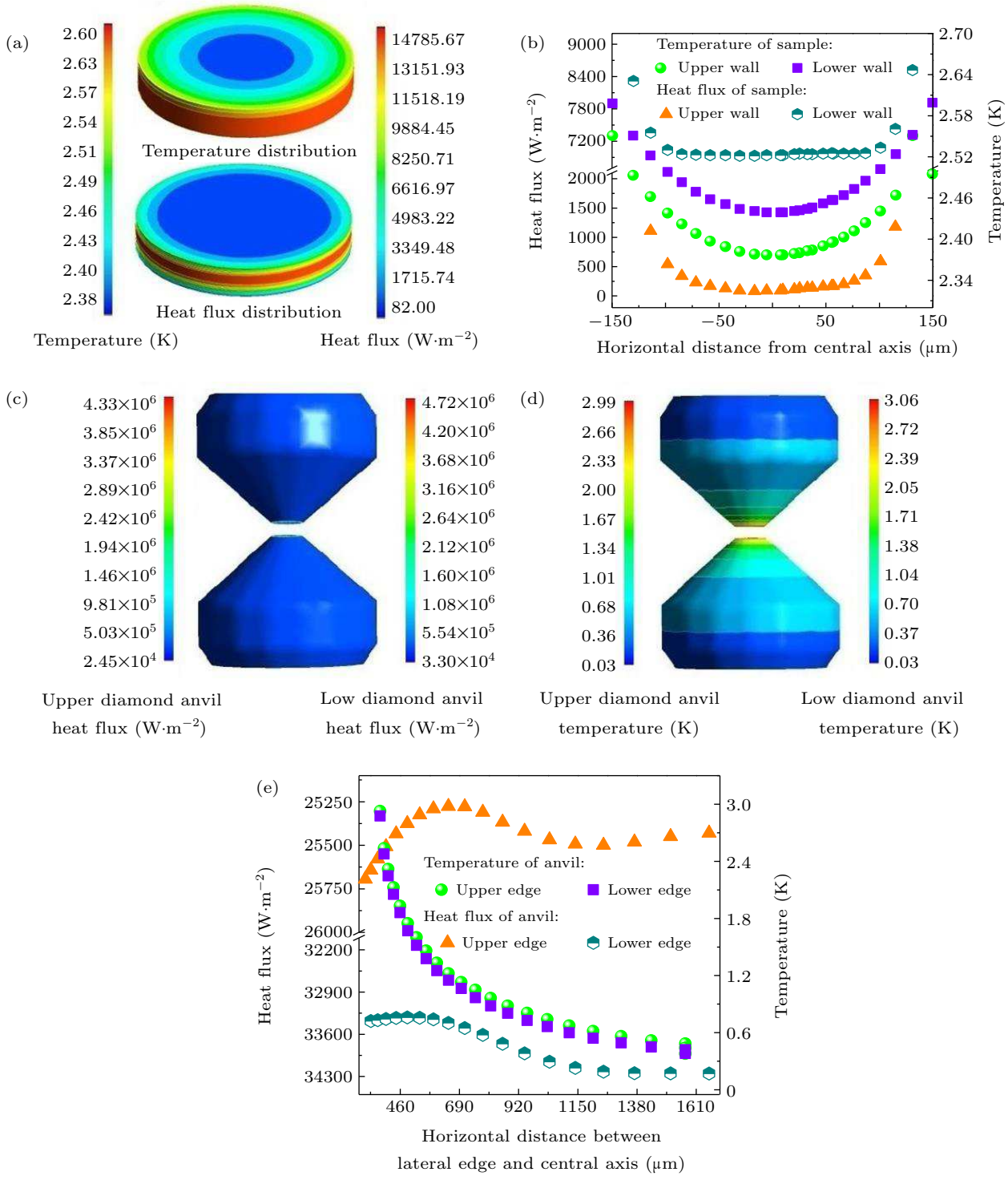


Fig. 2. The heat loss originating from the radiation effect. (a) Temperature and heat flux contours in the sample. (b) Temperature and heat flux distributions on the upper and lower walls of the sample. (c) Distribution of heat flux in DAs. (d) Temperature distributions in DAs. (e) Temperature heat flux profiles in DAs.

Due to the high thermal conductivity of diamond,[31] it is necessary to analyze the feedback sensitivity at the temperature measuring point when the thermal conductivity of the sample changes to illustrate the feasibility of measuring thermal conductivity for different materials by analyzing the temperature distribution in the DAC.

In order to study the temperature gradient of DAs under HT–HP conditions, two lateral lines at the edges were selected in the upper and lower DAs, as shown in Fig. 3(a). Then the temperature gradient of DAs for different samples with

different thermal conductivities, including 2 $W\cdot m^{-1}\cdot K^{-1}$, 20 $W\cdot m^{-1}\cdot K^{-1}$, 30 $W\cdot m^{-1}\cdot K^{-1}$, and 60 $W\cdot m^{-1}\cdot K^{-1}$, and different T_1–T_2 temperatures, including 873 K–903 K, 873 K–923 K, and 873 K–943 K, were simulated. Figure 3(b) shows the temperature distribution at 600 μm–1200 μm along the lateral edges of the upper and lower anvils for T_1–T_2 temperatures of 873 K–943 K and different thermal conductivities. When temperatures T_1–T_2 vary from 873 K–903 K to 873 K–943 K, and sample thermal conductivity is 2 $W\cdot m^{-1}\cdot K^{-1}$, the temperature gradient of the upper anvil varies from 1.8 K to 4.4 K, while the temperature gradient of the lower anvil varies from 8.1 K to 15.1 K. In this regard, figure 3(a) shows that as the temperature difference ΔT ($\Delta T = T_2 - T_1$) increases, the temperature gradient of the lateral edges of the DAs intensifies significantly. Moreover, figure 3(b) shows that for constant T_1 and T_2 temperatures in the bases of the upper and lower DAs, the temperature gradient of the lateral edges of the upper and lower DAs increases gradually with an increase in the thermal conductivity of the sample.

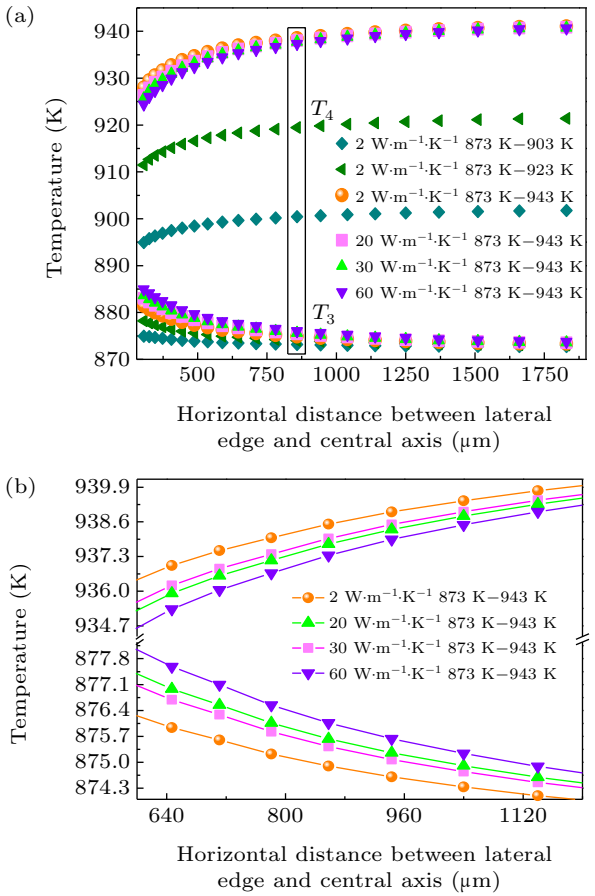


Fig. 3. (a) Temperature distribution along the lateral edges of the DAs. (b) Temperature distribution along the lateral edges of the DAs at 600 μm–1200 μm.

The midpoint positions D_3 and D_4 of the lateral edges of the DAs are defined as the positions where the temperature measurements were performed. Figure 4 shows the temperature distributions at measuring points D_3 and D_4 when the temperature T_1 is set to 873 K, while T_2 is set to 903 K, 923 K, and 943 K, respectively. When the sample thermal conductivity increases from 2 $W\cdot m^{-1}\cdot K^{-1}$ to 60 $W\cdot m^{-1}\cdot K^{-1}$ and T_1 and T_2 are constant, temperature T_3 varies from 874.6 K to 875.6 K at the midpoint position D_3 and temperature T_4 varies from 938.6 K to 937.7 K at the midpoint position D_4. Figure 4 indicates that variation of thermal conductivity of the sample is reflected in the temperature feedback at the temperature measurement point. Moreover, as the temperatures T_1 and T_2 increase, the sensitivity of temperature measurement at points D_3 and D_4 improves. Temperature variations at the measuring points D_3 and D_4 can also be observed in experiments in the form of variations of the thermal conductivity of the sample.

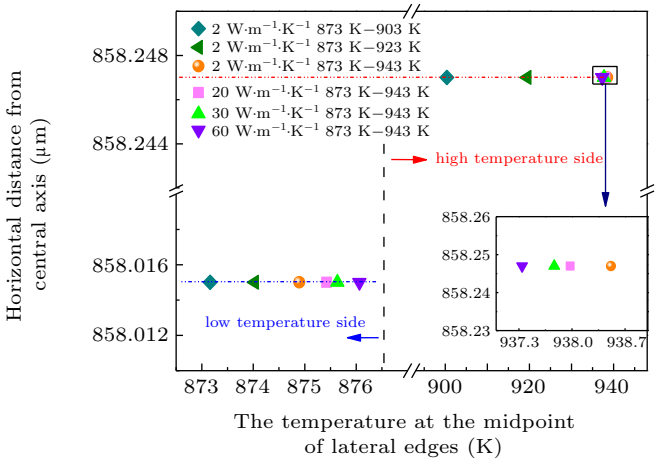


Fig. 4. Temperature distributions at the midpoint of the lateral edges of the DAs.

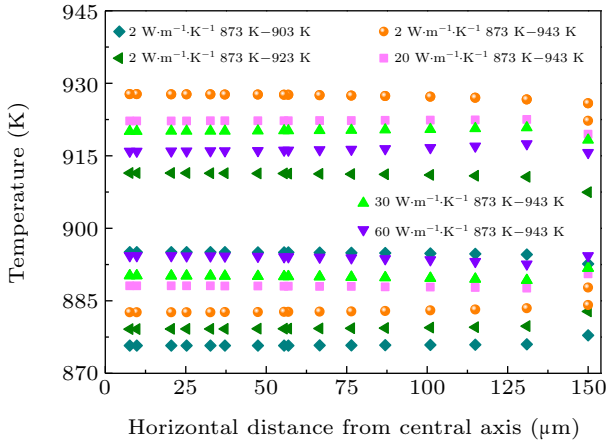


Fig. 5. Temperature distribution at the sample walls.

In order to observe the temperature distribution of the upper and lower walls of the sample in the DAC, figure 5 shows the temperature difference at different sample wall positions in the DAC. The horizontal temperature gradient on the surface of the sample subjected to steady-state heating is small. When the thermal conductivity of the sample is 20 $W\cdot m^{-1}\cdot K^{-1}$, temperatures of the upper and lower surfaces of the sample are 922.2 K–919.4 K and 888.1 K–890.5 K, respectively. Moreover, when the thermal conductivity of

the sample is 60 $W{\cdot}m^{-1}{\cdot}K^{-1}$, the temperatures of the upper and lower surfaces of the sample are 915.9 K–915.7 K and 894.3 K–894.4 K, respectively. Accordingly, it is found that when the sample thermal conductivity increases from 2 $W{\cdot}m^{-1}{\cdot}K^{-1}$ to 60 $W{\cdot}m^{-1}{\cdot}K^{-1}$, the maximum relative temperature error of the two ends and the middle position of the same surface of the sample is less than 2.5%. We can conclude that as the thermal conductivity of the sample increases, this relative temperature error decreases and the temperature of the upper/lower wall can be set to a certain value.

Accurate measurement of thermal conductivity by analysis of the temperature distribution in a DAC under high-pressure conditions has outstanding advantages. In this scheme, T_1–T_4 are the measured temperatures from four thermocouples. The measured temperatures T_1 and T_2 will be input to the FVM as boundary conditions. During the simulation, it was assumed that the thermal conductivity of the sample varies until the simulated temperatures t_3' and t_4' at the D_3 and D_4 reach the measured temperatures T_3 and T_4. Therefore, the input thermal conductivity reflects the real thermal conductivity of the sample. Figure S1 shows a flowchart for calculating the thermal conductivity of the sample in a DAC.

4. Conclusion

Studies show that the heat radiation effect has a great influence on the temperature distribution when the temperature gradient distribution of a DAC is realized by the steady-state method. In the present study, a coupled radiative–conductive heat transfer model is proposed to study the heat transport properties of samples in a DAC under HT–HP conditions. The main objective of this study was to avoid the influence of thermal radiation on the *in situ* thermal conductivity of the samples. To this end, the feasibility of investigating the thermal conductivity of different materials by combining the proposed numerical model with locally measured temperatures by thermocouples is discussed. Based on the obtained results, it is found that variations in the thermal conductivity of the sample have obvious temperature feedback at the temperature measurement point in the DAC, which has a certain guiding significance in the experiment. Combining the coupled numerical model with locally measured temperatures is an effective technical approach for simulating the temperature field, thermal conductivity and other thermal transport properties of the sample in a DAC under extreme HT–HP conditions. This paper is expected to provide a foundation for accurate measurement of *in situ* thermal conductivity in DACs under HT–HP conditions.

Acknowledgments

Project supported by the National Key Research and Development Program of China (Grant No. 2018YFA0702700) and the National Natural Science Foundation of China (Grant Nos. 11674404 and 11774126).

References

[1] Samudrala G K, Moore S L, Velisavljevic N, Georgiy M T, Paul A B and Yogesh K V 2016 *AIP Adv.* **6** 095027
[2] Sakai T, Yagi T, Ohfuji H, Irifune T, Ohishi Y, Hirao N, Suzuki Y, Kuroda Y, Asakawa T and Kanemura T 2015 *Rev. Sci. Instrum.* **86** 033905
[3] Natalia D, Leonid D, Razvan C and Michael H 2010 *Appl. Phys. Lett.* **97** 251903
[4] Liu S, Tang Q Q, Wu B B, Zhang F, Liu J Y, Fan C M and Lei L 2021 *Chin. Phys. B* **30** 016301
[5] Ji T T, Gao Y, Qin T R, Yue D H, Liu H, Han Y H and Gao C X 2021 *J. Phys. Chem. C* **125** 3314
[6] Huang Y P, Haung X L, Wang X, Zhang W T, Zhou D, Zhou Q, Liu B B and Cui T 2019 *Chin. Phys. B* **28** 096402
[7] Zhao L, Yue D H, Liu C L, Wang M, Han Y H and Gao C X 2019 *Chin. Phys. B* **28** 030702
[8] Li Y Q, Gao Y, Han Y H, Liu C L, Peng G, Wang Q L, Ke F, Ma Y Z and Gao C X 2015 *Appl. Phys. Lett.* **107** 142103
[9] Veksler I V and Hou T 2020 *Contrib. Mineral. Petrol.* **175** 1
[10] Li W M, Zhao J F, Cao L P, Hu Z, Huang Q Z, Wang X C, Liu Y, Zhao G Q, Zhang J, Liu Q Q, Yu R Z, Long Y W, Wu H, Lin H J, Chen C T, Li Z, Gong Z Z, Guguchia Z, Kim J S, Stewart G R, Uemura Y J, Uchida S and Jin C. Q 2019 *Proc. Natl. Acad. Sci. USA* **116** 12156
[11] Snider E, Dasenbrock-Gammon N, McBride R, Debessai M, Vindana H, Vencatasamy K, Lawler K V, Salamat A and Dias R P 2020 *Nature* **586** 373
[12] Shen G and Mao H K 2017 *Rep. Prog. Phys.* **80** 016101
[13] Hsieh W P, Zalden P, Wuttig M, Lindenberg A M and Mao W L 2013 *Appl. Phys. Lett.* **103** 191908
[14] Keller R and Holzapfe W B 1977 *Rev. Sci. Instrum.* **48** 517
[15] Stacey F D and Loper D E 2007 *Phys. Earth Planet. Interiors* **161** 13
[16] Marton F C, Shankland T J and Rubie D C 2005 *Phys. Earth Planet. Interiors* **149** 53
[17] Yue D H, Ji T T, Qin T R, Wang J, Liu C L, Jiao H, Zhao L, Han Y H, and Gao C X 2018 *Appl. Phys. Lett.* **112** 081901
[18] Pangilinan G I, Ladouceur H D and Russell T P 2000 *Rev. Sci. Instrum.* **71** 3846
[19] Shen G Y, Rivers M L, Wang Y B and Sutton S R 2001 *Rev. Sci. Instrum.* **72** 1273
[20] Yagi T, Ohta K and Kobayashi K 2011 *Meas. Sci. Technol.* **22** 024011
[21] Cahill D G, Chen B and Hsieh W P 2010 *Phys. Rev. B* **80** 180302
[22] Rainey E S G, Hernlund J W and Kavner A 2013 *J. Appl. Phys.* **114** 204905
[23] Beck P, Goncharov A F and Struzhkin V V 2007 *Appl. Phys. Lett.* **91** 181914
[24] Paolo D, Alessandro N and Daniele C 1998 *Appl. Opt.* **37** 5731
[25] Wang S, Ai Q, Zou T Q, Sun C and Xie M 2020 *Appl. Therm. Eng.* **177** 115457
[26] Taniguchi H, Ohmori T and Iwata M 2002 *Heat Transfer-Asian Research* **31** 391
[27] Powell R W, Tye R P and Woodman M J 1963 *J. Less-Common Met.* **5** 49
[28] Yue D H, Gao Y, Zhao L, Yan Y L, Tingting Ji T T, Han Y H and Chunxiao Gao 2019 *Jpn. J. Appl. Phys.* **58** 040906
[29] Nicolas M and Nicola M 2005 *Phys. Rev. B* **71** 205214
[30] Zhang H, Li Y M and Tao W Q 2017 *Appl. Therm. Eng.* **114** 337
[31] Olson J R, Pohl R O, Vandersande J W, Zoltan A, Anthony T R, and Banholzer W F 1993 *Phys. Rev. B* **47** 14850